HIGH-ENERGY RESUMMATION OF HIGGS p_{T} DISTRIBUTION*

Claudio Muselli

Tif Lab, Dipartimento di Fisica, Universitá di Milano
and INFN Sezione di Milano
Via Celoria 16, 20133 Milano, Italy
claudio.muselli@mi.infn.it

(Received March 28, 2017)

We discuss the generalization of high-energy resummation to transverse momentum distributions to leading-logarithmic accuracy. We check our procedure by reproducing the high-energy limit of the Feynman diagram calculations up to NLO to the Higgs production in gluon–gluon fusion. Then, we estimate finite top mass corrections to the NLO Higgs p_{T} distribution.

DOI:10.5506/APhysPolB.48.1105

1. Introduction

Resummation of leading high-energy (or small-x) contributions has a long story. These logs are logarithms of the ratio between the hard scale Q^2 of a particular process and the center-of-mass energy s. First pioneering works [1] showed how to take into account at all orders in α_{s} singular small-x terms into DGLAP evolution. Then, a general high-energy resummation theory in the case of inclusive cross sections at the first not trivial logarithmic order was proposed [2, 4]. In the following years, this theory was applied to resum leading small-x log (LLx) contributions for the most important processes in collider physics: heavy-quark photo- and lepto-production [2], deep-inelastic scattering [4], Standard Model [5, 6] and pseudo-scalar [7] Higgs production in gluon–gluon fusion, Drell–Yan [8], heavy-quarks production [9] and prompt-photon [10].

More recently, the resummation formalism was extended to the case of rapidity distributions in Ref. [11], through a different, but equivalent, approach to small-x resummation. This opens the possibility to study also exclusive observables which are more relevant from a phenomenological viewpoint.

* Presented at the Cracow Epiphany Conference "Particle Theory Meets the First Data from LHC Run 2", Kraków, Poland, January 9–12, 2017.

Following the same desire, in Ref. [12], a general high-energy resummation theory for transverse momentum distributions was developed. Besides being of theoretical and phenomenological interest, this extension represents another little step through a complete exclusive description of the desired final state. In the following, we present formulas for a generic hadro-initiated process, since generalization to lepto-, photo-initiated processes is very straightforward [12].

The main ingredient of small-x resummation is the so-called k_{T} factorization, *i.e.* the observation that in the high-energy regime any observable can be written as a convolution between a two-gluons irreducible hard part and two reducible ladders of emissions, as shown in Fig. 1 (on the right).

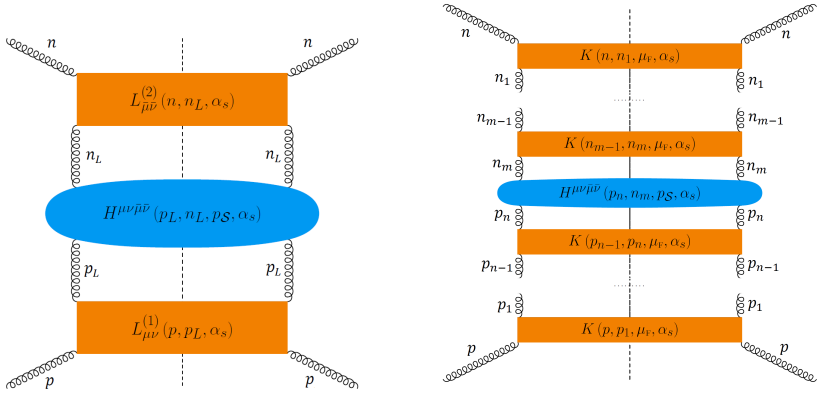

Fig. 1. On the right, k_{T} factorization for a general hadro-initiated observable into a process-dependent hard part and two ladders of radiation; on the left, decomposition of the ladder parts into multiple insertions of an emission kernel.

In the standard approach [2], k_{T} factorization of the hadronic total cross section σ is implemented as a convolution

$$\sigma\left(x, Q^2\right) = \int \frac{\mathrm{d}z}{z} \int \frac{\mathrm{d}\bar{z}}{\bar{z}} \int \frac{\mathrm{d}k_{\mathrm{T}}^2}{k_{\mathrm{T}}^2} \int \frac{\mathrm{d}\bar{k}_{\mathrm{T}}^2}{\bar{k}_{\mathrm{T}}^2} C\left(\frac{x}{z\bar{z}}, \frac{Q^2}{k_{\mathrm{T}}^2}, \frac{Q^2}{\bar{k}_{\mathrm{T}}^2}\right) \mathcal{G}\left(z, k_{\mathrm{T}}^2\right) \mathcal{G}\left(\bar{z}, \bar{k}_{\mathrm{T}}^2\right) \tag{1.1}$$

between a hard coefficient function C and two transverse momentum dependent gluon Green's functions. The convolution in Eq. (1.1) is performed on the longitudinal momentum fractions $z, \bar{z}$ and on the transverse momenta $k_{\mathrm{T}}, \bar{k}_{\mathrm{T}}$ of the two incoming gluons. High-energy resummation is then achieved by taking $\mathcal{G}$ as a solution of the BFKL equation. More in details, by taking a double Mellin transform w.r.t. x and Q^2, convolution of Eq. (1.1) factorizes into product

$$\sigma\left(N, M\right) = h\left(N, M, M\right) G\left(N, M\right) G\left(N, M\right) , \tag{1.2}$$

where the Mellin transforms are defined as

$$f\left(N, M_1, M_2\right) = \int_0^1 \mathrm{d}x\, x^{N-1} \int_0^\infty \mathrm{d}k_{\mathrm{T}}^2 \left(k_{\mathrm{T}}^2\right)^{M_1-1} \int \mathrm{d}\bar{k}_{\mathrm{T}}^2 \left(\bar{k}_{\mathrm{T}}^2\right)^{M_2-1} f\left(x, k_{\mathrm{T}}^2, \bar{k}_{\mathrm{T}}^2\right) \tag{1.3}$$

and $G(N, M)$ is the double Mellin transform of $\mathcal{G}$ divided by M. $h(N, M_1, M_2)$ is the double Mellin transform of the hard coefficient function C times M_1 and M_2

$$h\left(N, M_1, M_2\right) = M_1 M_2 \int_0^1 \mathrm{d}x\, x^{N-1} \int_0^\infty \mathrm{d}k_{\mathrm{T}}^2 \left(k_{\mathrm{T}}^2\right)^{M_1-1} \int \left(\bar{k}_{\mathrm{T}}^2\right)^{M_2-1} C\left(x, k_{\mathrm{T}}^2, \bar{k}_{\mathrm{T}}^2\right) \tag{1.4}$$

and it is called *impact factor*. Renormalization group equation for $G(N, M)$ gives the pole condition $M = \gamma_{\mathrm{s}}(\frac{\alpha_{\mathrm{s}}}{N})$ with γ_{s} the BFKL anomalous dimension, which resums pole of N, *i.e.* logarithms of x. Small-x resummation is then performed in N space as

$$\sigma^{\mathrm{res}}\left(N, Q^2\right) = h\left(N, \gamma_{\mathrm{s}}\left(\frac{\alpha_{\mathrm{s}}}{N}\right), \gamma_{\mathrm{s}}\left(\frac{\alpha_{\mathrm{s}}}{N}\right)\right) . \tag{1.5}$$

In Ref. [11], instead, a different approach was proposed. Starting from k_{T} factorization, the reducible ladder part was computed through the iteration of a collinear safe kernel γ, as depicted in Fig. 1 (on the left). In conclusion, the cross section for n emissions from the upper leg and m emissions from the lower leg is computed by n, m insertions of a radiation kernel γ following by a subtraction of the first $n-1$, $m-1$ collinear poles according to $\overline{\mathrm{MS}}$ prescription. For inclusive cross section, this brings to the following resummed expression:

$$\begin{aligned} \sigma^{\mathrm{res}}\left(N, Q^2\right) \;=\; & \sum_{n,m} \sigma_{n,m} = \gamma\left(N, \alpha_{\mathrm{s}}\right)^2 \int_0^\infty \mathrm{d}k_{\mathrm{T}}^2 \left(k_{\mathrm{T}}^2\right)^{\gamma(N,\alpha_{\mathrm{s}})-1} \\ & \times \int_0^\infty \mathrm{d}\bar{k}_{\mathrm{T}}^2 \left(\bar{k}_{\mathrm{T}}^2\right)^{\gamma(N,\alpha_{\mathrm{s}})-1} C\left(N, k_{\mathrm{T}}^2, \bar{k}_{\mathrm{T}}^2\right) R\left(N, \alpha_{\mathrm{s}}\right)^2 , \end{aligned} \tag{1.6}$$

where the only difference with Eq. (1.5) is the scheme-dependent factor R which takes into account that subtraction was performed in $\overline{\mathrm{MS}}$ scheme. In this approach, non-trivial information is encoded in the kernel γ. High-energy resummation is then achieved by choosing γ to be the dual [13] of the BFKL kernel (at the first order $\gamma = \gamma_{\mathrm{s}}$).

The generalized ladder approach of Ref. [11] permits to move from inclusive observable to more exclusive one since the complete kinematic of radiation is calculable and under control. In the context of high-energy resummation of transverse momentum distribution, it can be proved that Eq. (1.6) still holds, as long as the hard coefficient function C is substituted with a transverse momentum dependent hard function C_{p_T}.

This proceeding will be structured as following: in the next section, the general framework of high-energy resummation of transverse momentum distribution will be briefly summarized. Then, using the EFT Higgs boson production as test process, we are going to check the conclusion of the theory against a fixed order calculation. Then, in the last section, we will discuss high-energy phenomenology for the Higgs p_T distribution both in EFT case and with complete dependence from the quark masses.

2. Transverse momentum distribution at high energy

Now we are going to briefly sketch the important points in the derivation of the high-energy resummation theory for transverse momentum distributions. Our aim in this section is to highlight the key steps which permits such a resummation rather than clarify all the mathematical subtleties. For the complete proof, we refer the reader to the original paper, Ref. [12].

The starting point, as said before in the introduction, is k_T factorization. Figure 2 represents a general factorize observable. Black point in each emission stands for an insertion of the radiation kernel $\gamma(N, \alpha_\mathrm{s})$, while the grey/red circle represents the transverse momentum dependent two-gluon irreducible observable. Moreover, we decide to call $\mathcal{S}$ the desired final state which we want to study with complete dependence from its transverse momentum.

The main feature of this approach is the possibility to study the complete kinematic of the process. However, it is important to stress that if we are interested to resum at LLx a particular observable of a tagged final state $\mathcal{S}$, we need to integrate over all the phase space of the other radiation. Therefore, it is not possible to be differential also in the rapidity or in the transverse momentum of some gluon emitted in the ladders (momenta $q_i, \dots, q_\mathrm{L}$ and $r_j, \dots, r_\mathrm{L}$ of Fig. 2).

If all the transverse momenta of the gluons in the ladders are integrated out, we are not considering angular correlation between them, and transverse momentum p_T of the desired final state $\mathcal{S}$ is going to depend only from the momenta of the gluons exiting the ladders (p_L and n_L of Fig. 2). Therefore, multiple insertions of the collinear kernel $\gamma(N, \alpha_\mathrm{s})$ and next $\overline{\mathrm{MS}}$ subtractions go as in the inclusive total cross-section case.

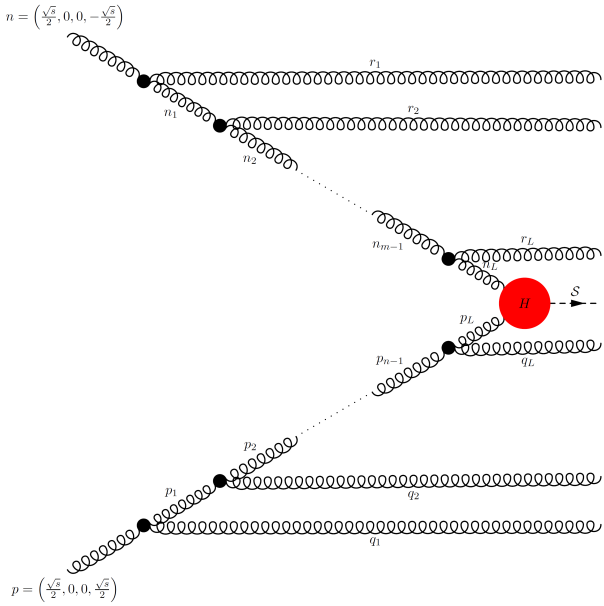

Fig. 2. Kinematics of the ladders. The blob at each emission vertex denotes inclusion of LLx s- and t-channel gluon radiation to all orders.

In conclusion, the LLx resummed transverse momentum distribution of a particular process is evaluated by the following formula in N space:

$$\frac{\mathrm{d}\sigma^{\mathrm{res}}}{\mathrm{d}p_{\mathrm{T}}^2}\left(N, p_{\mathrm{T}}^2\right) = \gamma\left(N, \alpha_{\mathrm{s}}\right)^2 R\left(N, \alpha_{\mathrm{s}}\right)^2 \int_0^\infty \mathrm{d}k_{\mathrm{T}}^2 \left(k_{\mathrm{T}}^2\right)^{\gamma(N,\alpha_{\mathrm{s}})-1} \times \int_0^\infty \mathrm{d}\bar{k}_{\mathrm{T}}^2 \left(\bar{k}_{\mathrm{T}}^2\right)^{\gamma(N,\alpha_{\mathrm{s}})-1} C_{p_{\mathrm{T}}}\left(N, k_{\mathrm{T}}^2, \bar{k}_{\mathrm{T}}^2, p_{\mathrm{T}}^2\right), \quad (2.1)$$

where k_{T} and $\bar{k}_{\mathrm{T}}$ are the modulus of the transverse momenta of the gluons p_{L} and n_{L} and $C_{p_{\mathrm{T}}}$ is the LO transverse momentum distribution of the off-shell process

$$g^* + g^* \to \mathcal{S}\,. \quad (2.2)$$

Another important point we want to focus on is the following: $C_{p_{\mathrm{T}}}$ represents the process-dependent part of this resummation and it is an LO observable of an off-shell process. It is not important if the on-shell limit of such observable exists; if it is zero or does not exist, the resummed observable Eq. (2.1), expanded in powers of α_{s}, will start one order higher than $C_{p_{\mathrm{T}}}$, implicitly requiring that at least one gluon must be emitted in the ladders.

This property of high-energy resummation is very useful since very often the LO observable for the off-shell process is simpler than putting off-shell the LO on-shell diagrams.

We are going to clarify all these concepts by presenting the resummation for a particular process: the Higgs boson production in gluon–gluon fusion in the effective field theory.

In the case of Higgs boson production in the limit when the top mass tends to infinity, we consider the Higgs coupled directly to gluons through an effective vertex. However, being a 2 to 1 process, if we require a non-vanishing transverse momentum, we need the radiation of at least one additional gluon. Hence, the LO on-shell process is the $2 \to 2$ process

$$g + g \to H + g(q)\,. \tag{2.3}$$

Nevertheless, as said before, to perform the high-energy resummation of this observable, we need to compute the transverse momentum distribution of

$$g^* + g^* \to H \tag{2.4}$$

rather than the off-shell version of Eq. (2.3)

$$g^* + g^* \to H + g(q)\,, \tag{2.5}$$

since transverse dependence of process Eq. (2.4) is also not trivial without any further emission.

The transverse momentum dependent hard function $C_{p_\mathrm{T}}(N, k_\mathrm{T}^2, \bar{k}_\mathrm{T}^2, p_\mathrm{T}^2)$ turns out to be

$$\begin{aligned} C_{p_\mathrm{T}}\left(N, k_\mathrm{T}^2, \bar{k}_\mathrm{T}^2, p_\mathrm{T}^2\right) \;=\; & \frac{1}{m_H^2} \frac{2\sigma_0}{\left(1 + \frac{p_\mathrm{T}^2}{m_H^2}\right)^N} \\ & \times \int_0^{2\pi} \frac{\mathrm{d}\theta}{2\pi} \cos^2\theta \delta\left(p_\mathrm{T}^2 - k_\mathrm{T}^2 - \bar{k}_\mathrm{T}^2 - 2k_\mathrm{T}\bar{k}_\mathrm{T}\cos\theta\right), \end{aligned} \tag{2.6}$$

where k_T, $\bar{k}_\mathrm{T}$ and p_T are the transverse momenta of the incoming gluons and of the Higgs, respectively, N is the Mellin variable associated to x,

$$\sigma_0 = \frac{G_F m_H^2 \alpha_\mathrm{s}^2 \sqrt{2}}{576\pi} \tag{2.7}$$

and θ is the angle between the direction of $\boldsymbol{k}$ and $\bar{\boldsymbol{k}}$.

Now by inserting the expression of $C_{p_{\mathrm{T}}}$, Eq. (2.6), into Eq. (2.1) and solving the integrals [12], we come to the resummed expression for the transverse momentum distribution of the Higgs in the framework of the effective theory

$$\frac{\mathrm{d}\sigma^{\mathrm{res}}}{\mathrm{d}\xi_p}\left(N, p_{\mathrm{T}}^2\right) = R\left(\gamma\left(N,\alpha_{\mathrm{s}}\right)\right)^2 \sigma_0 \frac{\xi_p^{2\gamma(N,\alpha_{\mathrm{s}})-1}}{\left(1+\xi_p\right)^N} \times \left[\frac{\Gamma\left(1+\gamma\left(N,\alpha_{\mathrm{s}}\right)\right)^2 \Gamma\left(2-2\gamma\left(N,\alpha_{\mathrm{s}}\right)\right)}{\Gamma\left(2-\gamma\left(N,\alpha_{\mathrm{s}}\right)\right)^2 \Gamma\left(2\gamma\left(N,\alpha_{\mathrm{s}}\right)\right)}\left(1+\frac{2\gamma\left(N,\alpha_{\mathrm{s}}\right)^2}{1-2\gamma\left(N,\alpha_{\mathrm{s}}\right)}\right)\right], \quad (2.8)$$

where we introduce $\xi_p = \frac{p_{\mathrm{T}}^2}{m_H^2}$.

Through the identification in Eq. (2.8) of $\gamma(N,\alpha_{\mathrm{s}})$ with the dual of the BFKL kernel $\gamma(N,\alpha_{\mathrm{s}}) = \gamma_{\mathrm{s}}(\frac{\alpha_{\mathrm{s}}}{N})$, we are finally able to resum at LLx this observable.

However, to provide tests of the following construction, before turning to phenomenology, we want to check the expansion in power of α_{s} of Eq. (2.8) against fixed order evaluation. This will be the subject of the following subsection. We are going to present a fixed order evaluation directly in the high-energy limit: this will permit us to compute completely analytical expressions up to $\mathcal{O}(\alpha_{\mathrm{s}}^4)$[1].

2.1. Fixed order calculation at high energy

We start by computing the α_{s}-expansion of Eq. (2.8) up to $\mathcal{O}(\alpha_{\mathrm{s}}^4)$. The BFKL anomalous dimension admits the following expansion:

$$\gamma_{\mathrm{s}}\left(\frac{\alpha_{\mathrm{s}}}{N}\right) = \frac{N_{\mathrm{c}}\alpha_{\mathrm{s}}}{\pi}\frac{1}{N} + \mathcal{O}\left(\alpha_{\mathrm{s}}^4\right), \quad (2.9)$$

while the R factor which takes into account the $\overline{\mathrm{MS}}$ scheme selection begins to be different from 1 at $\mathcal{O}(\alpha_{\mathrm{s}}^3)$

$$R\left(\gamma_{\mathrm{s}}\left(\alpha_{\mathrm{s}}, N\right)\right) = 1 + \mathcal{O}\left(\alpha_{\mathrm{s}}^3\right). \quad (2.10)$$

Using this information, the expansion of Eq. (2.8) at a non-zero value of ξ_p turns out to be, in the limit when $N \to 0$

$$\frac{\mathrm{d}\sigma}{\mathrm{d}\xi_p}\left(N,\xi_p\right) = \sigma_0\left[\frac{2\bar{\alpha}_{\mathrm{s}}}{N}\frac{1}{\xi_p} + \frac{4\bar{\alpha}_{\mathrm{s}}{}^2}{N^2}\frac{\ln\xi_p}{\xi_p} + \mathcal{O}\left(\alpha_{\mathrm{s}}^3\right)\right] + \mathcal{O}\left(\alpha_{\mathrm{s}}^4\right) \quad (2.11)$$

[1] In the original paper Ref. [12], the comparison at $\mathcal{O}(\alpha_{\mathrm{s}}^4)$ was presented only through a numerical integration over rapidity of the full double differential fixed order evaluation of Ref. [14].

with

$$\bar{\alpha_{\rm s}} = \frac{\alpha_{\rm s} N_{\rm c}}{\pi} \,. \tag{2.12}$$

It is interesting to note that the expansion starts at $\mathcal{O}(\alpha_{\rm s}^3)$, while $C_{p_{\rm T}}$ is of $\mathcal{O}(\alpha_{\rm s}^2)$ (see Eqs. (2.6), (2.7)). This is due to the fact that the on-shell limit of the off-shell process, Eq. (2.4), is zero at finite $p_{\rm T}$, as noted before.

We now want to reproduce this expansion by computing directly Feynman diagrams at small-x. At $\mathcal{O}(\alpha_{\rm s}^3)$, we have to compute only the following subprocess:

$$g + g \to H + g \tag{2.13}$$

since radiation of quarks is a subleading effect [12]. Diagrams which we have to evaluate are collected in Fig. 3, with a useful light-cone decomposition for the momenta of the various particle. When $x \to 0$, the LLx behaviour is dominated by the region when $\bar{z}, z \ll 1$ and $\frac{k_{\rm T}^2}{s}, \frac{\bar{k}_{\rm T}^2}{s} \ll 1$. In this region, the contribution of the first diagram of Fig. 3 turn out to be in $d = 4 - 2\epsilon$ dimension

$$\frac{{\rm d}\sigma_{0-{\rm a}}}{{\rm d}\xi_p}(x, \xi_p) = \sigma_0 \frac{\bar{z}}{x} \delta\left(1 - \frac{\bar{z}}{x} + \bar{\xi}\right) \left[\bar{\alpha_{\rm s}} \frac{{\rm d}\bar{z}}{\bar{z}} \frac{{\rm d}\bar{\xi}}{\bar{\xi}^{1+\epsilon}} \frac{4\pi}{\Gamma(1-\epsilon)}\right] \delta\left(\xi_p - \bar{\xi}\right) \tag{2.14}$$

with $\bar{\xi} = \frac{\bar{k}_{\rm T}^2}{m_H^2}$ and $\bar{\alpha_{\rm s}}$, σ_0 defined as in Eqs. (2.12) and (2.7). By solving integrations over $\bar{z}$ and $\bar{\xi}$ using the two delta constraints and by taking the limit $\epsilon \to 0$, we find the result for the single emission from the upper leg

$$\frac{{\rm d}\sigma_{0-{\rm a}}}{{\rm d}\xi_p}(x, \xi_p) = \sigma_0 \bar{\alpha_{\rm s}} \frac{1}{\xi_p} \,. \tag{2.15}$$

Since the contribution from the other leg is the same by symmetry and due to the fact that interferences between emissions are subleading in the high-energy regime, we can easily come to our final result for the $\mathcal{O}\left(\alpha_{\rm s}^3\right)$ (in the Mellin space)

$$\frac{{\rm d}\sigma_0}{{\rm d}\xi_p}(N, \xi_p) = 2\sigma_0 \bar{\alpha_{\rm s}} \frac{1}{\xi_p} \int_0^1 {\rm d}x\, x^{N-1} = \sigma_0 \frac{2\bar{\alpha_{\rm s}}}{N} \frac{1}{\xi_p} \tag{2.16}$$

as predicted by Eq. (2.11).

Now we move to $\mathcal{O}(\alpha_{\rm s}^4)$. In this case, we have to evaluate three contributions (see Fig. 4): when the two emissions of gluons come from the upper leg or from the lower leg or when they are one from the upper leg and one from the lower leg. Clearly, as before, due to symmetry the first two contributions are exactly equal.

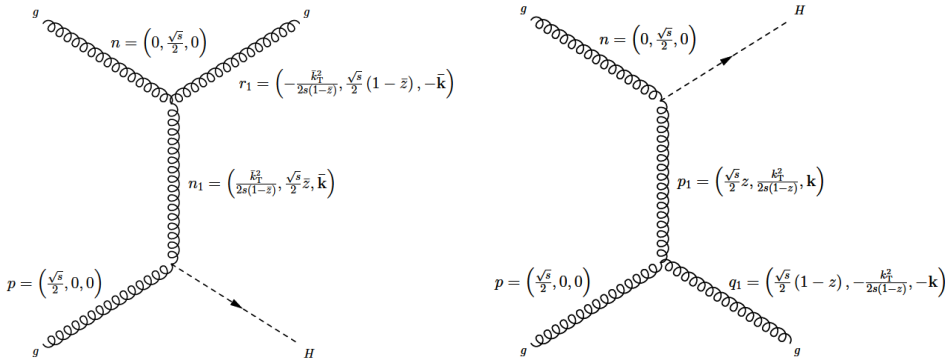

Fig. 3. Feynman diagrams contributing at $\mathcal{O}(\alpha_{\mathrm{s}}^3)$. A useful light-cone decomposition for the momenta is also reported.

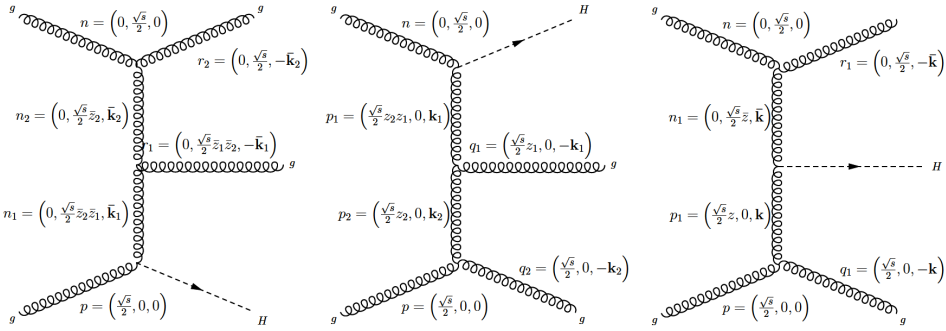

Fig. 4. Feynman diagrams contributing at $\mathcal{O}(\alpha_{\mathrm{s}}^4)$, with light-cone decomposition for the momenta in the high-energy regime. It can be proved that in the small-x limit at this order in α_{s}, $k_{\mathrm{T}1}^2 \gg k_{\mathrm{T}2}^2$ [11, 12].

We start by considering the case of a double emissions from the same leg. Since angular correlations can be shown to be subleading at small-x, from now on we will neglect all of them. Consequently, we will omit all angular terms like $\frac{(4\pi)^\epsilon}{\Gamma(1-\epsilon)}$ as they are always subtracted in the $\overline{\mathrm{MS}}$ scheme [11]. At small-x, the result for the differential cross section is

$$\frac{\mathrm{d}\sigma_{1-\mathrm{a}}}{\mathrm{d}\xi_p}(x,\xi_p) = \sigma_0 \frac{\bar{z}_1\bar{z}_2}{x}\delta\left(1-\frac{\bar{z}_1\bar{z}_2}{x}+\bar{\xi}_1\right)\left[\bar{\alpha}_{\mathrm{s}}\frac{\mathrm{d}\bar{z}_2}{\bar{z}_2}\frac{\mathrm{d}\bar{\xi}_2}{\bar{\xi}_2^{1+\epsilon}}\right]\left[\bar{\alpha}_{\mathrm{s}}\frac{\mathrm{d}\bar{z}_1}{\bar{z}_1}\frac{\mathrm{d}\bar{\xi}_1}{\bar{\xi}_1^{1+\epsilon}}\right]\delta\left(\xi_p-\bar{\xi}_1\right) . \tag{2.17}$$

Now, using the two delta constraints we solve the integration over $\bar{z}_1$ and $\bar{\xi}_1$ obtaining at LLx

$$\frac{\mathrm{d}\sigma_{1-\mathrm{a}}}{\mathrm{d}\xi_p}(x,\xi_p) = \sigma_0 \bar{\alpha}_{\mathrm{s}}{}^2 \left[\int_x^1 \frac{\mathrm{d}\bar{z}_1}{\bar{z}_1} \int_0^{\xi_p} \frac{\mathrm{d}\bar{\xi}_2}{\bar{\xi}_2}\right] \frac{1}{\xi_p^{1+\epsilon}} + \mathcal{O}(1)$$
$$= \sigma_0 \bar{\alpha}_{\mathrm{s}}{}^2 \ln\frac{1}{x}\left[-\frac{1}{\epsilon}\frac{1}{\xi_p^{1+2\epsilon}}\right] + \mathcal{O}(1)\,. \tag{2.18}$$

Last step is to take the small-ϵ limit and perform the $\overline{\mathrm{MS}}$ subtraction. At finite p_{T}, we obtain

$$\frac{\mathrm{d}\sigma_{1-\mathrm{a}}}{\mathrm{d}\xi_p}(x,\xi_p) = \sigma_0 \bar{\alpha}_{\mathrm{s}}{}^2 \ln\frac{1}{x}\frac{\ln\xi_p}{\xi_p}\,. \tag{2.19}$$

Equation (2.19) is also the result for the double radiation from the lower leg. To conclude our check, we need to add the term coming from the diagram in which the two emissions are one for each leg. In this case, the differential cross section in the high-energy regime is

$$\frac{\mathrm{d}\sigma_{1-\mathrm{c}}}{\mathrm{d}\xi_p}(x,\xi_p) = \frac{\sigma_0}{2}\frac{\bar{z}z}{x}\delta\left(1-\frac{\bar{z}z}{x}+\xi_p\right)\left[\bar{\alpha}_{\mathrm{s}}\frac{\mathrm{d}z}{z}\frac{\mathrm{d}\xi}{\xi^{1+\epsilon}}\right]\left[\bar{\alpha}_{\mathrm{s}}\frac{\mathrm{d}\bar{z}}{\bar{z}}\frac{\mathrm{d}\bar{\xi}}{\bar{\xi}^{1+\epsilon}}\right]\frac{\mathrm{d}\theta}{2\pi}$$
$$\times\delta\left(\xi_p-\xi-\bar{\xi}-2\sqrt{\bar{\xi}\xi}\cos\theta\right)\,, \tag{2.20}$$

where θ, as in Eq. (2.6), is the angle between the direction of the momenta $\boldsymbol{k}$ and $\bar{\boldsymbol{k}}$. To solve the various integrations, we first note that Eq. (2.20) is symmetric by exchanging ξ with $\bar{\xi}$. Hence, we can halve the integration region by requiring $\xi > \bar{\xi}$ and recover the other part by exploting the symmetry. Then, we perform the following change of variables:

$$\bar{\xi} = \xi_p\, w\, \xi_1\,, \qquad \xi = \xi_p\,\xi_1\,, \qquad \cos\theta = t\,. \tag{2.21}$$

We thus write Eq. (2.20) as, by ignoring terms beyond LLx

$$\frac{\mathrm{d}\sigma_{1-\mathrm{c}}}{\mathrm{d}\xi_p}(N,\xi_p) = \sigma_0 \bar{\alpha}_{\mathrm{s}}{}^2 \int_x^1 \frac{\mathrm{d}z}{z}\frac{1}{\xi_p^{1+2\epsilon}}\int_{-1}^1 \frac{\mathrm{d}t}{\sqrt{1-t^2}}\int_0^1 \mathrm{d}w \frac{(1+w+2\sqrt{w}t)^{2\epsilon}}{w^{1+\epsilon}} + \mathcal{O}(1)\,. \tag{2.22}$$

Finally, we perform the expansion $\epsilon \to 0$ and the $\overline{\mathrm{MS}}$ subtraction to obtain

$$\frac{\mathrm{d}\sigma_{1-\mathrm{c}}}{\mathrm{d}\xi_p}(x,\xi_p) = 2\sigma_0 \bar{\alpha}_{\mathrm{s}}{}^2 \ln\frac{1}{x}\frac{\ln\xi_p}{\xi_p}\,. \tag{2.23}$$

Putting together Eq. (2.19) with Eq. (2.23), we then arrive to the complete $\mathcal{O}(\alpha_{\mathrm{s}}^4)$ prediction in the small-x limit (in the Mellin space)

$$\frac{\mathrm{d}\sigma_1}{\mathrm{d}\xi_p}(N,\xi_p) = 4\sigma_0\bar{\alpha_{\mathrm{s}}}^2\frac{\ln\xi_p}{\xi_p}\int_0^1 \mathrm{d}x\, x^{N-1}\ln\frac{1}{x} = \sigma_0\frac{4\bar{\alpha_{\mathrm{s}}}^2}{N^2}\frac{\ln\xi_p}{\xi_p} \tag{2.24}$$

in agreement with the expansion of the high-energy resummed formula (2.11).

Hence, we have reproduced the first orders of the expansion through an explicit computation of the Feynman diagrams in the high-energy limit, providing another check on the resummed construction. Being our theory on solid ground, we are now able to discuss some phenomenological application of the technique. Next section will be devoted to the study of mass quark effects on the p_{T} distribution of the Higgs.

3. Higgs p_{T} distribution: Phenomenology

We now turn to study the phenomenological implication of our high-energy resummation on the p_{T} distribution of Higgs boson production.

In the previous section, Higgs boson production in gluon fusion at high energy was evaluated in the effective field theory limit. This general formalism can be applied to the same observable, but now retaining full heavy-quark mass dependence. Such a calculation was performed in Ref. [15]. We want now to review these results and use them to qualitatively estimate mass corrections beyond leading order.

It is well-known that the impact of high-energy resummation is quite small at the current work energies of LHC Run 2. However, in cases when fixed order evaluation is not available, α_{s}-expansion of the resummed result can be used to extract qualitatively information about the behaviour of the unknown coefficient.

Hence, in this section, we are first going to validate this high-energy approximation at LO and NLO at the hadronic level and then to provide a prediction for the transverse momentum distribution at NLO with complete mass quark dependence based on the high-energy approximation.

High-energy resummation predicts a very different behaviour at large-p_{T} between the pointlike case (as in the effective field theory limit) and the resolved case (as with full heavy-quark mass dependence) [12]. While when the interaction is pointlike, the coefficients grow logarithmically with p_{T} (ξ_p), in the resolved case, the coefficients $d_k(\xi_p)$ as $\xi_p \to \infty$ will vanish at least as an extra power of ξ_p^{-1} in such a way that the integral over all transverse momenta is finite. In formulas

$$\frac{\mathrm{d}\sigma}{\mathrm{d}\xi_p} \underset{x\to 0}{\sim} \frac{\sigma_{\mathrm{LO}}}{\xi_p} \times \begin{cases} \displaystyle\sum_{k=1}^{\infty} \alpha_{\mathrm{s}}^k \ln^{k-1} \frac{1}{x} \sum_{n=0}^{k-1} c_{kn} \ln^n \xi_p \,, & \text{pointlike}\,, \qquad (3.1a) \\ \displaystyle\sum_{k=1}^{\infty} \mathrm{d}_k\left(\xi_p\right) \alpha_{\mathrm{s}}^k \ln^{k-1} \frac{1}{x} \,, & \text{resolved}\,. \qquad (3.1b) \end{cases}$$

For this reason, the high-energy approximation is the right approximation to study mass quark effects in the large-p_{T} region, when the EFT approximation badly fails.

All plots are produced with $\mu_{\mathrm{R}}^2 = \mu_{\mathrm{F}}^2 = Q^2$ and with the PDF4LHC15 NNLO set of parton distributions PDF4LHC15_nnlo_100 [16]. Q^2 is a p_{T}-dependent hard scale

$$Q^2 = \left(\sqrt{m_H^2 + p_{\mathrm{T}}^2} + p_{\mathrm{T}}\right)^2 ; \qquad (3.2)$$

with this choice of hard scale, hadronic transverse momentum distribution is returned by a standard convolution between the partonic distribution and a p_{T}-independent PDF luminosity [15].

We start from the validation of the high-energy expansion, by comparing with the known fixed order full result. We define a high-energy approximation by taking the expansion of our resummed prediction as

$$\begin{aligned} \frac{\mathrm{d}\sigma^{\mathrm{res}}}{\mathrm{d}\xi_p}\left(\tau, \xi_p\right) &= \frac{\mathrm{d}\sigma_0^{\mathrm{he}}}{\mathrm{d}\xi_p}\left(\tau, \xi_p\right) \alpha_{\mathrm{s}}^3 + \frac{\mathrm{d}\sigma_1^{\mathrm{he}}}{\mathrm{d}\xi_p}\left(\tau, \xi_p\right) \alpha_{\mathrm{s}}^4 + \mathcal{O}\left(\alpha_{\mathrm{s}}^5\right) \\ &= \frac{\mathrm{d}\sigma_0^{\mathrm{he}}}{\mathrm{d}\xi_p}\left(\tau, \xi_p\right) \alpha_{\mathrm{s}}^3 \left(1 + \alpha_{\mathrm{s}} K^{(1),\mathrm{he}}\left(\tau, \xi_p\right)\right) , \qquad (3.3) \end{aligned}$$

where in the second line, we have also defined the NLO K-factor. In Fig. 5, we show several comparisons — two for $\frac{\mathrm{d}\sigma_0^{\mathrm{he}}}{\mathrm{d}\xi_p}$ and two for $\frac{\mathrm{d}\sigma_1^{\mathrm{he}}}{\mathrm{d}\xi_p}$. In the upper left panel, we show the ratio between the LO EFT and the LO EFT high-energy approximation, in the upper right panel, the ratio between the full mass-dependent LO result and its high-energy approximation. The ratio with the full LO pointlike is also shown. Both these plots are computed at LHC 13 TeV. In the lower panels, we show the validation at NLO at LHC 13 TeV (on the left) and for a wide range in p_{T} and $\sqrt{s}$ (on the right)[2].

These plots show that high-energy approximation, even if it is accurate only at very high center-of-mass energy, much higher than the current work energies at the LHC Run 2, it is quite stable in a large range of p_{T}. At the

[2] Comparing with the original Ref. [15], in the contour plot, we double the grid of points near the kinematic boundary to obtain more accurate results. However, at the moment, this region is inaccessible for present colliders.

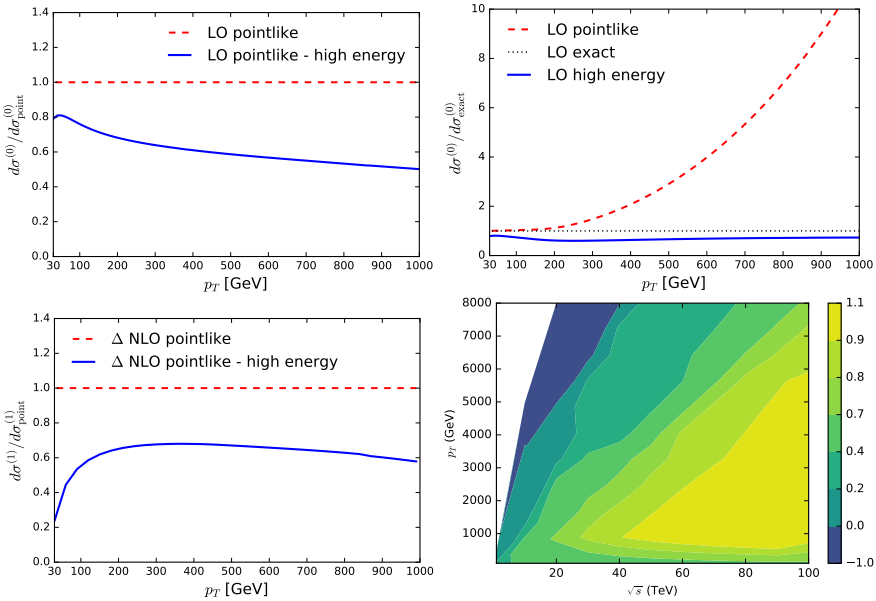

Fig. 5. Several comparisons for high-energy approximation validation. In the upper panels, comparisons between LO full coefficient and LO high-energy approximation both in the EFT and with full masses dependence are shown. In the lower panels, we validate at NLO high-energy approximation by comparing EFT full result with its high-energy expansion, at 13 TeV (on the right) and in a wide range of both p_{T} and $\sqrt{s}$ (on the left).

LHC 13 TeV, at LO, it is about 60% of the full theory, and only slightly worse at NLO. On the contrary, the effective field theory result is driven by the fact that at the parton level, it has the wrong large-p_{T} power behaviour, and it is off by an increasingly large factor: already for $\sqrt{s} = 13$ TeV at $p_{\mathrm{T}} \sim 1$ TeV, it is in fact too large by about one order of magnitude.

By comparing results at LO at LHC 13 TeV obtained in EFT or in full theory (left panels of Fig. 5), it is clear that the quality of the high-energy approximation is similar in both cases. Due to this observation, where only EFT exact result is available, we expect the accuracy, we extract by the pointlike comparison, may be used as a good estimator of the uncertainty also in the massive case.

Moreover, the contour plot of Fig. 5 shows that the high-energy approximation becomes better as the center-of-mass energy is increased at fixed p_{T} but also, if p_{T} is varied at fixed energy, that the quality of the approximation remains constant in a wide range of transverse momenta. It only starts deteriorating when the transverse momentum becomes of the same order of its upper kinematic limit $\frac{\sqrt{s}}{2}$. This is expected because the high-energy limit holds when $\sqrt{s}$ is much larger than all other scales: remember that

in the derivation of the high-energy regime in the previous section, we have considered the limit

$$\frac{p_{\mathrm{T}}^2}{s} \ll 1\,. \tag{3.4}$$

Logs of this ratio, which are subleading at small-x, might be important at very large p_{T} and should be resummed to all orders [17]. However, in this region, the transverse momentum distribution is tiny, so, in practice, the high-energy approximation is uniformly accurate throughout the physically relevant region.

We now finally turn to the p_{T} spectrum of the Higgs boson with finite quark masses effects beyond leading order at LHC 13 TeV. In Fig. 6, three different determination of the K-factor, Eq. (3.3) are plotted in the high-p_{T} region we are interested in: using the full pointlike NLO result or the high-energy approximation both in EFT and with full mass dependence. In each case, both the LO and NLO contributions are computed using the same approximation. This plot suggests two main conclusions. First, by comparing dashed (red) line *vs.* dot-dashed (green) line, namely EFT full result against high-energy approximation of it, we see our expansion at small-x is quite good, with an accuracy of about 20% or better for all $p_{\mathrm{T}} \gtrsim 200$ GeV, in agreement with the general validation just exposed. Second, even though the shape of the distribution (see Eqs. (3.1a), (3.1b)) at high p_{T} differs between the pointlike and massive case (a different power of p_{T}), the K-factors are similar and approximately p_{T} independent, at least, in the only case in which we can compare the pointlike and massive results, namely the high-energy limit (dot-dashed (green), *vs.* solid curves (blue)).

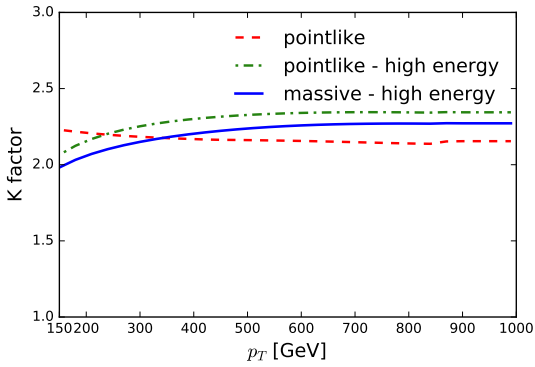

Fig. 6. (Colour on-line) Various approximations to the NLO Higgs transverse momentum distribution K-factor: using NLO and LO pointlike full coefficients (dashed/red), the NLO and LO pointlike high-energy approximation (dot-dashed/green) or the NLO and LO full mass dependent high-energy approximation (solid/blue).

From Fig. 6, we can also extract one of the conclusions of this proceeding. If one wishes to use the NLO pointlike result to approximate the real Higgs p_{T} distribution, a better approximation can be obtained by using the pointlike NLO to compute the K-factor and using it to rescale the full massive leading order rather than to add to it.

Indeed, the quality of this approximation is possibly comparable to that obtained by summing the LO full massive coefficient with the high-energy approximation of the NLO, as you can appreciate from Fig. 7.

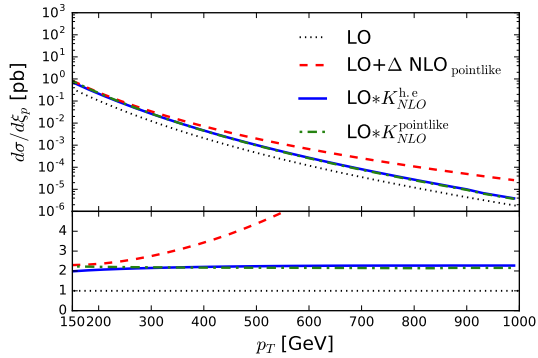

Fig. 7. Various approximation to the NLO Higgs transverse momentum distribution. Colours and line styles follow the same definition of Fig. 6.

4. Conclusions and outlook

We have reported on an extension of high-energy factorisation to transverse momentum distributions. It represents a further step in a more exclusive description of the final state in the high-energy regime. Moreover, we reproduce order by order in α_{s} the high-energy limit through a direct evaluation of Feynman diagrams in the small-x limit. As a first application, we have performed the resummation of the p_{T} distribution for Higgs production in gluon–gluon fusion, both with finite quark masses and in the infinite mass limit. Using this information, we estimate the impact of quark masses corrections on the Higgs NLO p_{T} distribution at LHC 13 TeV. We found that even if the full NLO pointlike result is off by an increasingly large factor for $p_{\mathrm{T}} \gtrsim 200$ GeV, the pointlike K-factor is of the same order as the prediction computed using full massive high-energy expansion. Hence, full massive LO result rescaled by pointlike NLO K-factor can be used to obtain a reasonable approximation for the unknown massive NLO correction of the Higgs p_{T} distribution.

A better understanding of such effects can be obtained by matching the high-energy resummation with other known resummations. Matching procedures with threshold resummation or transverse momentum resummation

are under studies [18, 19]. Even a more exclusive extension of the high-energy resummation technique (such as high-energy resummation double differential in rapidity and transverse momentum) is highly desirable.

REFERENCES

[1] L.N. Lipatov, *Sov. J. Nucl. Phys.* **23**, 338 (1976) [*Yad. Fiz.* **23**, 642 (1976)]; V.S. Fadin, E.A. Kuraev, L.N. Lipatov, *Phys. Lett. B* **60**, 50 (1975).

[2] S. Catani, M. Ciafaloni, F. Hautmann, *Phys. Lett. B* **242**, 97 (1990).

[3] S. Catani, M. Ciafaloni, F. Hautmann, *Nucl. Phys. B* **366**, 135 (1991).

[4] S. Catani, F. Hautmann, *Nucl. Phys. B* **427**, 475 (1994) [arXiv:hep-ph/9405388].

[5] F. Hautmann, *Phys. Lett. B* **535**, 159 (2002) [arXiv:hep-ph/0203140].

[6] S. Marzani *et al.*, *Nucl. Phys. B* **800**, 127 (2008) [arXiv:0801.2544 [hep-ph]].

[7] S. Marzani *et al.*, *Nucl. Phys. Proc. Suppl.* **186**, 98 (2009) [arXiv:0809.4934 [hep-ph]].

[8] S. Marzani, R.D. Ball, *Nucl. Phys. B* **814**, 246 (2009) [arXiv:0812.3602 [hep-ph]].

[9] R.D. Ball, R.K. Ellis, *J. High Energy Phys.* **0105**, 053 (2001) [arXiv:hep-ph/0101199].

[10] G. Diana, *Nucl. Phys. B* **824**, 154 (2010) [arXiv:0906.4159 [hep-ph]].

[11] F. Caola, S. Forte, S. Marzani, *Nucl. Phys. B* **846**, 167 (2011) [arXiv:1010.2743 [hep-ph]].

[12] S. Forte, C. Muselli, *J. High Energy Phys.* **1603**, 122 (2016) [arXiv:1511.05561 [hep-ph]].

[13] G. Altarelli, R.D. Ball, S. Forte, *Nucl. Phys. B* **575**, 313 (2000) [arXiv:hep-ph/9911273].

[14] C.J. Glosser, C.R. Schmidt, *J. High Energy Phys.* **0212**, 016 (2002) [arXiv:hep-ph/0209248].

[15] F. Caola *et al.*, *J. High Energy Phys.* **1608**, 150 (2016) [arXiv:1606.04100 [hep-ph]].

[16] J. Butterworth *et al.*, *J. Phys. G* **43**, 023001 (2016) . [arXiv:1510.03865 [hep-ph]].

[17] E.L. Berger, J.w. Qiu, X.f. Zhang, *Phys. Rev. D* **65**, 034006 (2002) [arXiv:hep-ph/0107309].

[18] S. Marzani, *Phys. Rev. D* **93**, 054047 (2016) [arXiv:1511.06039 [hep-ph]].

[19] C. Muselli, S. Forte, G. Ridolfi, *J. High Energy Phys.* **0317**, 106 (2017) [arXiv:1701.01464 [hep-ph]].